Mechanical Behavior of Post-processed Inconel 718 Manufactured Through the Electron Beam Melting Process

by

Michael M. Kirka[1,2], Frank Medina[3], and Ryan Dehoff[1,2], Alfred Okello[1,2]

[1]Manufacturing Demonstration Facility, Oak Ridge National Laboratory, Knoxville, TN
[2]Materials Science & Technology Division, Oak Ridge National Laboratory, Oak Ridge, TN
[3]Arcam AB, Mölndal, Sweden

*corresponding author: email: kirkamm@ornl.gov, tel: 1-865-574-1094

Abstract

The electron beam melting (EBM) process was used to fabricate Inconel 718. The microstructure and tensile properties were characterized in both the as-fabricated and post-processed state transverse (T-orientation) and longitudinal (L-orientation) to the build direction. Post-processing involved both a hot isostatic pressing (HIP) and solution treatment and aging (STA) to homogenize the microstructure. In the as-fabricated state, EBM Inconel 718 exhibits a spatially dependent microstructure that is a function of build height. Spanning the last few layers is a cored dendritic structure comprised of the products (carbides and Laves phase) predicted under equilibrium solidification conditions. With increasing distance from the build's top surface, the cored dendritic structure becomes increasingly homogeneous with complete dissolution of the secondary dendrite arms. Further, temporal phase kinetics are observed to lead to the dissolution of the strengthening γ" and precipitation of networks of fine δ needles that span the grains. Microstructurally, post-processing resulted in dissolution of the δ networks and homogeneous precipitation of γ" throughout the height of the build. In the as-fabricated state, the monotonic tensile behavior exhibits a height sensitivity within the T-orientation at both 20 and 650 °C. Along the L-orientation, the tensile behavior exhibits strength values comparable to the reference wrought material in the fully heat-treated state. After post-processing, the yield strength, ultimate strength, and elongation at failure for the EBM Inconel 718 were observed to have beneficially increased compared to the

Notice of Copyright This manuscript has been authored by UT-Battelle, LLC under Contract No. DE-AC05-00OR22725 with the U.S. Department of Energy. The United States Government retains and the publisher, by accepting the article for publication, acknowledges that the United States Government retains a non-exclusive, paid-up, irrevocable, world-wide license to publish or reproduce the published form of this manuscript, or allow others to do so, for United States Government purposes. The Department of Energy will provide public access to these results of federally sponsored research in accordance with the DOE Public Access Plan (http://energy.gov/downloads/doe-public-access-plan).

as-fabricated material. Further, as a result of post-processing the spatial variance of the ultimate yield strength and elongation at failure within the transverse direction decreased by 4 and 3x respectively.

1 Introduction

Inconel 718 is the most widely used nickel-base (Ni-base) superalloy by the aerospace community despite being first developed in the 1960s [1,2]. The usage of Inconel 718 can be directly attributed to the excellent mechanical properties and corrosion resistance at temperatures up to 650 °C [3,4]. The strength exhibited by Inconel 718 directly related to the precipitation and size of the strengthening γ". However, due to the metastable nature of the primary strengthening phase (γ") in the alloy and ability for undesirable phases to form, heat-treatment (HT) of Inconel 718 can be difficult [2,5]. Further, heat-treatment of Inconel 718 is generally optimized for the intended material/component environment or service conditions [2].

Due to Inconel 718's workhorse status, there exists much interest in fabricating high temperature service components through additive manufacturing (AM) processes due to the large degree of design flexibility offered by the technology. Inconel 718 has been processed by selective laser melting (SLM), electron beam melting (EBM), and laser engineering net shaping (LENS) [6–10]. However, due to AM being an emerging family of technologies, the degree to which AM processing conditions (high solidification rates, high thermal gradients) effect the materials is not widely understood. Further, relatively few studies have reported the effects of post-processing on AM fabricated Inconel 718 and the associated impacts on the microstructure and mechanical properties of the material [7,8,11,12].

In the present study, Inconel 718 is fabricated by EBM. Characterized is the microstructure and mechanical properties of the EBM Inconel 718 in the as-fabricated state and after undergoing a combined hot isostatic pressure (HIP) and solution and aging treatment. Ultimately, the intent of this study is to provide further insight into the behavior of AM processed high temperature alloys and the manners through which their properties can be enhanced.

2 Experimental Procedure and Methods

The feedstock material was plasma wire atomized Inconel 718 manufactured by Advanced Powders and Coatings (Quebec, Canada). The powder feedstock was comprised of particles with a size distribution of 40-120μm (-100+325 mesh). Further particles were highly spherical and contained minimal internal porosity as illustrated in Figure 1. The nominal chemical composition is given in Table 1.

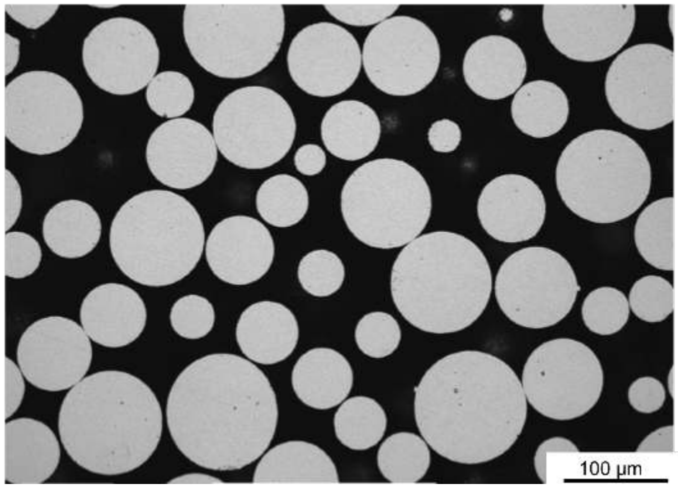

Figure 1: SEM micrograph AP&C Inconel 718 powder used in this study.

An Arcam A2X EBM machine was used to additively build a series of prismatic blocks (100x100x20 mm) and cylinders (⌀15x100 mm)with a diameter of 15 mm and height of 100 mm as shown in Figure 2. The start plate used was a 150x150x10 mm, 304L stainless steel start plate. The A2X was equipped with EBM Control V4.1 controls software. Within EBM Control, the prismatic geometries were loaded as a group rather than independent pieces while a raster scan pattern was used by the beam to melt. Within the Arcam software, beam velocity and current are a function of line scan length and speed function [13]. In the present work, a speed function of 63 was used. With the advance of each layer the control algorithm rotated the scan direction by 90°. The build began once a preheat temperature of 975 $^{\circ}$C was achieved. The electron gun accelerating voltage was set to 60 kV. For the build, a layer thickness of 75 μm was used.

Table 1: Nominal chemical compositions of the Inconel 718 powder used in this work given as weight percent.

Cr	Fe	Nb	Mo	Ti	Cu	Al	C	Ni
18.5	18.5	5	3	1	0.15	0.5	0.05	Bal

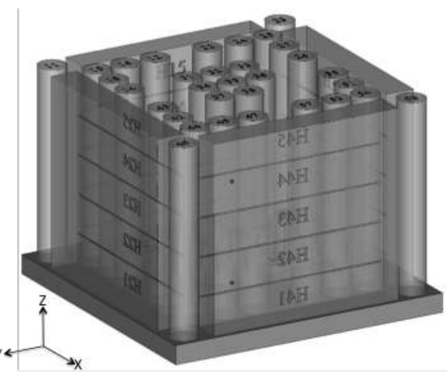

Figure 2: Computer generated representation of build fabricated in this work.

After completion of the build, half of the samples were given a two-step post-processing treatment comprised of hot isostatic pressing (HIP) and solution treatment and aging (STA). The material was HIP'd at a temperature of 1200 °C and 100 MPa for 240 minutes. The following STA was given to the EBM material: solutioning at 1066 °C for 80 minutes, followed by a double aging at 760 °C for 10 hours, and subsequent cool-down and aging at 650 °C for 10 hours. These STA conditions were chosen to be similar to those traditionally processed Inconel 718 are given [14].

Illustrated in Figure 3 is the association of the terminology transverse orientation (T-orientation) and longitudinal orientation (L-orientation) in relation to the build direction. Specimens for monotonic tensile testing were machined from the prismatic blocks transverse to the build direction. From each block, five specimen blanks were removed with a center-to-center spacing of 15 mm. A single specimen was taken aligned longitudinal to the direction of the build from each of the cylinders. The specimens were machined into a cylindrical dogbone geometry with a gauge diameter of 5.6 mm and gage length of 42 mm. Monotonic tensile experiments were conducted according to ASTM E8-13a for room temperature testing and ASTM E21-09 for testing at 650 °C [15, 16]. In all cases, the tensile experiments were done in open air conditions and at a strain rate of 0.005 $\frac{1}{min}$. High temperature tensile experiments were conducted using a Mayes elevated temperature extensometer (Model: R3/8 Block 2) on a Instron load frame equipped with a 250 kN load cell. Room temperature testing was conducted using an Instron 5582 load frame equipped with a 100 kN load cell and a Instron model 2620 extensometer.

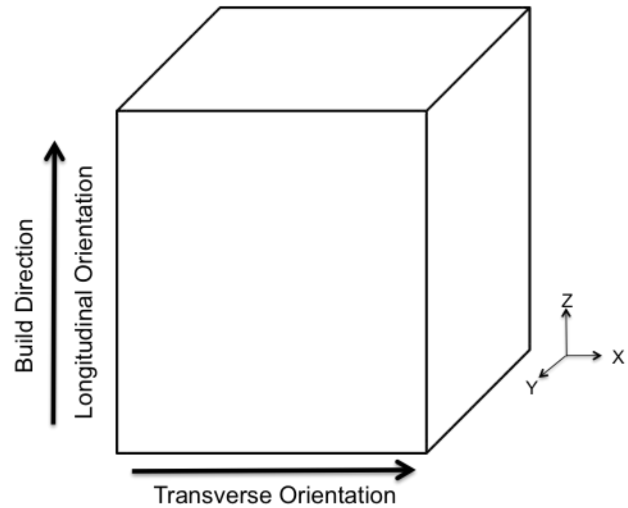

Figure 3: Schematic depicting the orientation relationship between the build direction and the longitudinal and transverse material orientations.

Samples were sectioned using an Allied High Tech TECHCUT 5 and mounted in KonductoMet using a Buehler SimpliMet XPS1. The mounted samples were metallographically prepared using successively finer silica carbide grinding paper and given a final polish with 1 μm diamond on an Allied High Tech MetPrep 4. Chemical etching via submersion using a mixture of HCL, acetic acid, and HNO_3 (1:1:1) was used to reveal the microstructure. Microscopy was conducted using a Leica DM4000M optical microscope and a Hitachi S4800 field emission scanning electron microscope. Electron back scatter detection (EBSD) was done using a JEOL 6500 field emission scanning electron microscope equipped with a EDAX Hikari EBSD camera.

3 Results and Discussion

3.1 As-built Microstructure

Comprising the bulk microstructure of the as-fabricated Inconel 718 utilized in this study are columnar grains aligned parallel to the build direction as depicted in Figure 4. The epitaxial solidification is attributable to alignment of the thermal gradient with the build direction [17–19]. However, complicating the understanding of the as-fabricated material is the impact of the variation in time at temperature each material point within the build experiences in relation to the solid-solid state phase transformations that occur within the material. As a result, the process-structure relationships are sensitive and unique to the combination of build geometry/layout in addition to processing parameters [9,20]. A more detailed study of the as-fabricated material is discussed elsewhere and summarized below for reference and comparison to the post-processed material [21].

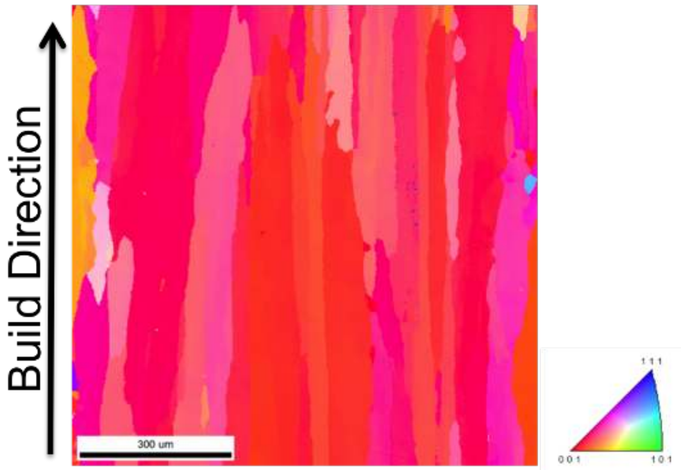

Figure 4: Grain orientation map depicting the columnar grains of EBM Inconel 718 in the as-fabricated state.

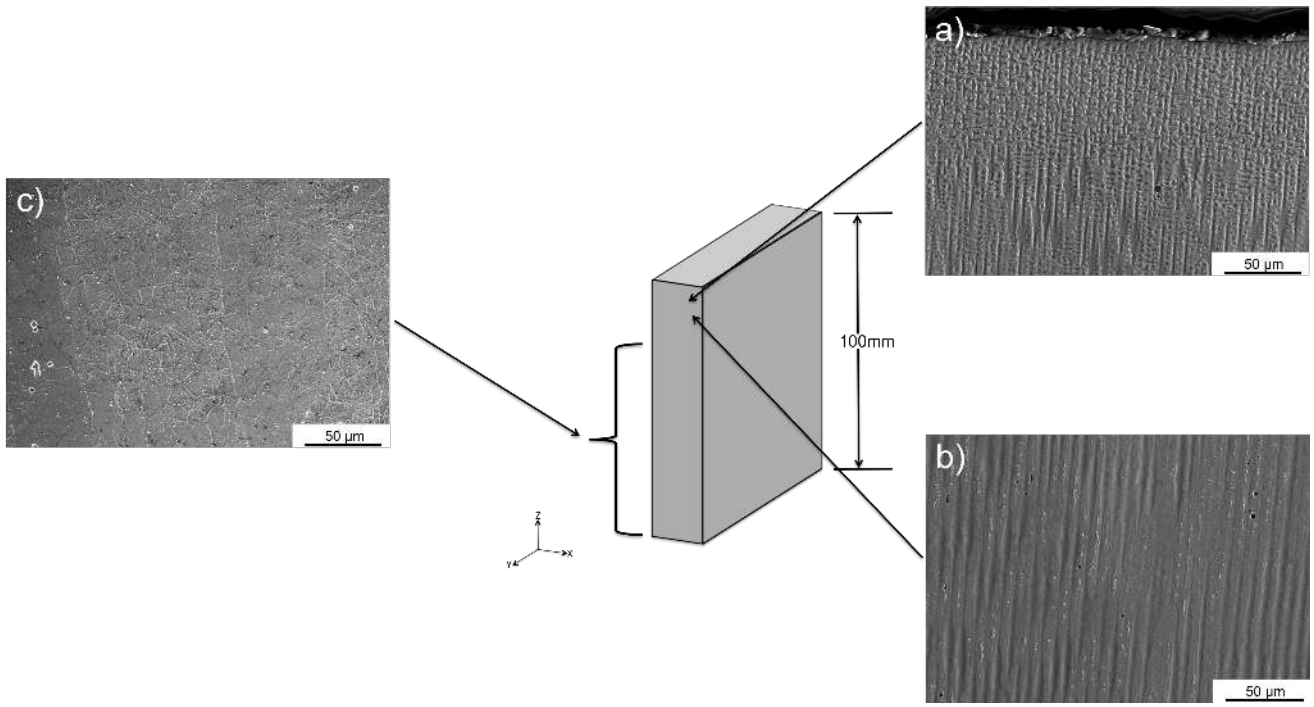

Figure 5: Spatial variation of the as-fabricated Inconel 718 EBM microstructure a) Dendritic structure near the top of the build b) Diffuse dendritic microstructure occuring ≈ 2 mm from the build top c) Representative bulk microstructure starting 5 mm from the top of the build.

As a function of build height, the phase distribution and precipitate sizes of the as-fabricated EBM Inconel 718 exhibits a spatial dependence as illustrated in Figures 5a-c. While the quantifiable microstructure attributes are specific to this build, the general observations of the spatially dependent microstructure discussed here still hold for EBM Inconel 718 material fabricated in other builds. Across the last few layers, the dendritic structure is retained (Figure 5a), with the interdendritic regions containing Laves phase and niobium rich carbides (Figure 6) [21]. Further, γ" 80 nm in size are observed in the γ matrix in the final layers of the build. The presence of the γ" in the final layer the build can be attributed to precipitation of γ" on cool-down after completion of the build due to the temperature sensitive γ" precipitation kinetics requiring a minimum of 600 seconds for precipitation at 850°C under the most optimal conditions [22–24]. Overall, the additional precipitate phases observed in the interdendritic regions can be considered consistent with the four step solidification sequence described by Knorovsky et al. [25] in their study of cast Inconel 718.

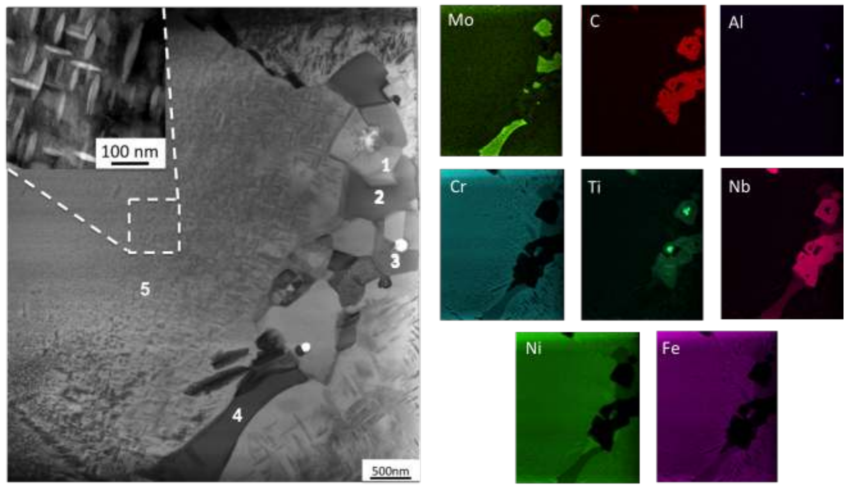

Figure 6: TEM micrograph of the matrix and interdenritic regions as viewed within the plane of the build in the second to last layer [21].

With increasing distance away from the top of the build, the dendritic structure gradually homogenizes as evidenced by loss of the secondary dendrite arms as illustrated in Figure 5b. Homogenization of the microstructure can be attributed to the time spent by the material at temperature during the build process [26–28]. At locations once occupied by the interdendritic Laves phase, small needle δ are observed to have precipitated. This can be attributed to the concentration of niobium in the interdendritic regions with the dissolution of the metastable Laves phase. Further, as the metastable γ" decomposes with increasing thermal exposure, fine scale networks of spurious δ ($\approx$ 100nm in size) precipitate throughout the matrix as illustrated in Figure 7a. Towards the bottom of the build, the γ" size is measured to be on average of 35 nm, however this is sensitive to the specific build conditions. Further, in the areas immediately surrounding the δ that has precipitated are regions of the matrix denude of γ".

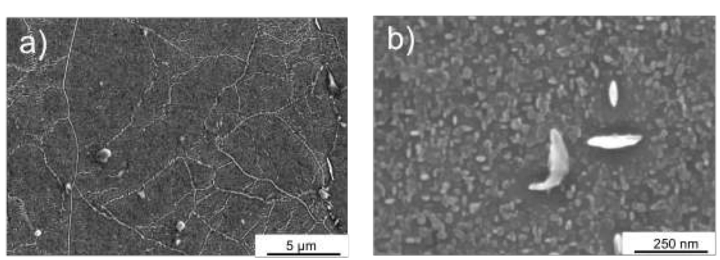

Figure 7: Representative micrographs of Inconel 718 in the bulk material in the as-fabricated state magnifying a) The spurious networks of δ precipitates crossing the grains depicted in Figure 5c b) The γ" precipitates with denuded zones surrounding δ precipitates.

Comparatively, microstructures reported for laser and EBM processed Inconel 718 have lacked the presence of the spurious δ networks (Figure 7a) observed here. Rather δ was reported to form as needles protruding from interdendritic and grain boundary regions [6,29,30]. Based on a combination of elemental heterogeneity and temperature, different morphological forms of δ are kinetically favored [3, 31, 32]. Additionally, chemical banding of δ has been reported by Strondl et al. [30] and Sames [33], however, in the case of the present Inconel 718 material this was not observed. In the few cases where chemical banding has been reported, δ was in the form of long needles ($\approx$ 25-50 μm) that span the width of grains [29, 33]. In the case of Inconel 718 processed through SLM, metastable products such as Laves phase and chemical segregation are observed.

3.2 Post-processed Microstructure

Inconel 718 is a precipitate strengthened Ni-base superalloy, whose mechanical properties are sensitive to phase fractions and precipitate sizes. As a result, heat-treatments are often highly specialized to account for both the process through which the Inconel 718 was manufactured and the intended operating conditions of the material [2, 34–36]. Further, optimizing the HT for a range of precipitate structures obtainable in Inconel 718 is difficult due to the rapid γ" coarsening rates and the low solvus temperature of Inconel 718 [2]. Concerning AM Inconel 718, relatively few studies have considered the effects of HT on the as-fabricated microstructures and corresponding mechanical behavior [7].

Unlike previously reported occurrences of recrystallization in post-processing of EBM Inconel 718, the post-process treatment used here retained the columnar grains of the as-fabricated microstructure as shown in Figure 8 [37]. Interestingly, both the HIP and STA conditions used in this work are similar to the ones utilized by Unocic et al. [37], however, the initial microstructure in their work was comprised of large δ needles over 100μm in length. Traditionally, δ is considered to be a grain size controlling phase ASM Handbook [38]. However, carbides have also been reported to serve a similar roll as δ in Inconel 718. Further, residual stress can also be considered a driver for recrystallization. However, neutron radiography has shown the residual stress in EBM Inconel 718 to be minimal compared to laser Inconel 718 [39]. This can be largely attributed to the time Inconel 718 spends at temperature during the EBM build process.

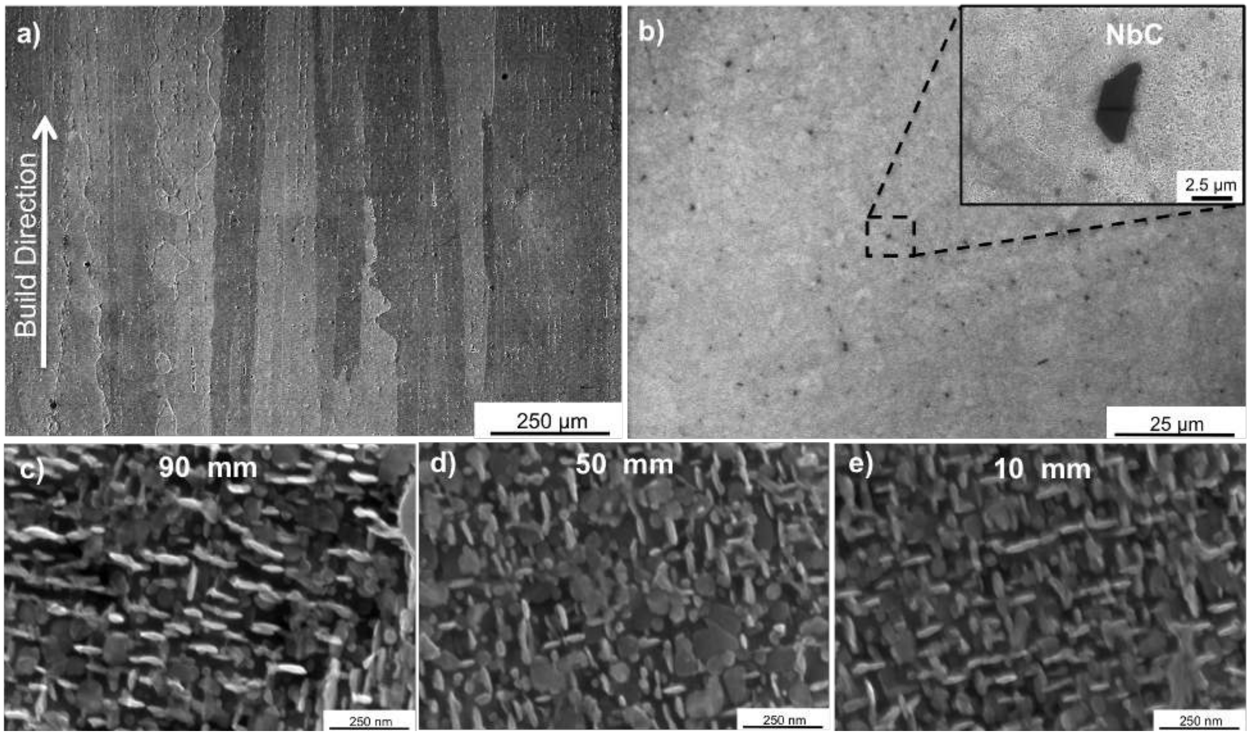

Figure 8: SEM micrograph of the post-processed Inconel 718 microstructure a) Depicting the retention of the columnar grain structure at 100X b) Uniformity of the γ matrix with a dismemberment of Niobium-rich carbides at 1,000X c) γ" 90 mm away from the bottom of the build at 100,000X d) γ" 50 mm away from the bottom of the build at 100,000X e) γ" 10 mm away from the bottom of the build at 100,000X.

The resultant post-processed EBM Inconel 718 microstructure is illustrated in Figure 8a-e. Through the combination of the HIP and STA, the spurious globular and needle like δ of the as-fabricated microstructure was placed into solution as can be seen by comparing Figures 8b and 5c. As reported by Cai et al. [40], exposure of forged Inconel 718 to 1020 °C and 120 minutes is sufficient to bring about a 9% dissolution of δ by volume fraction. Based on the dissolution kinetics of δ, the thermal exposure during the HIP'ing step of the post-process route taken here can be assumed to have brought about the complete dissolution of the δ in the material. Additionally, the phase make-up within the γ matrix is uniformly representative spanning the 100 mm build height as illustrated by Figures 8c-e. While not observed here, Qi et al. [41] have reported the mass transformation of Laves into globular δ as a result of STA treatment.

In their work Zhang et al. [8] solution annealed Inconel 718 fabricated with SLM at 1080 °C which resulted in the retention of the characteristic columnar grains, with the additional precipitation of acicular δ along the grain boundaries. However, in a similar approach, Chlebus et al. [7] reported solution annealing of SLM fabricated Inconel 718 at temperatures above 1040 °C resulted in recrystalization of the material.

3.3 Tensile Properties

Presented in Figure 9a-d is the stress-strain behavior of the as-fabricated EBM Inconel 718 in the L and T-directions in relation to HT wrought Inconel 718 at 20 and 650 °C. Overall, the as-fabricated EBM Inconel 718 exhibits similar hardening behavior as the wrought material despite the presence of largely columnar grains. However, the transverse properties (Figure 9c-d) exhibit a sensitivity to build height at both 20 and 650 °C with the yield strength (σ_{YS}) and ultimate tensile strength (σ_{UT}) exhibiting rages of $\approx$ 50 MPa and $\approx$ 160 MPa respectively, with the elongation at failure (ϵ_f) spanning 3-20%. In general, for the transverse tensile behavior of the as-fabricated Inconel 718 is strongest nearest the top of the build, with both the yield and ultimate tensile strength progressively declining with distance away from the top of the build. Within the L-orientation, the yield strength and ultimate tensile strength exhibit a strength variation of ±20MPa. The variability in ϵ_f in the T-orientation can be attributed to material defects such as entrapped porosity aligned along columnar grain boundaries. Strondl et al. [29] in their work on EBM Inconel 718 reported sensitivity of the tensile properties to build orientation, similarly entrapped stringer porosity aligned along the build direction was cited as the controlling factor.

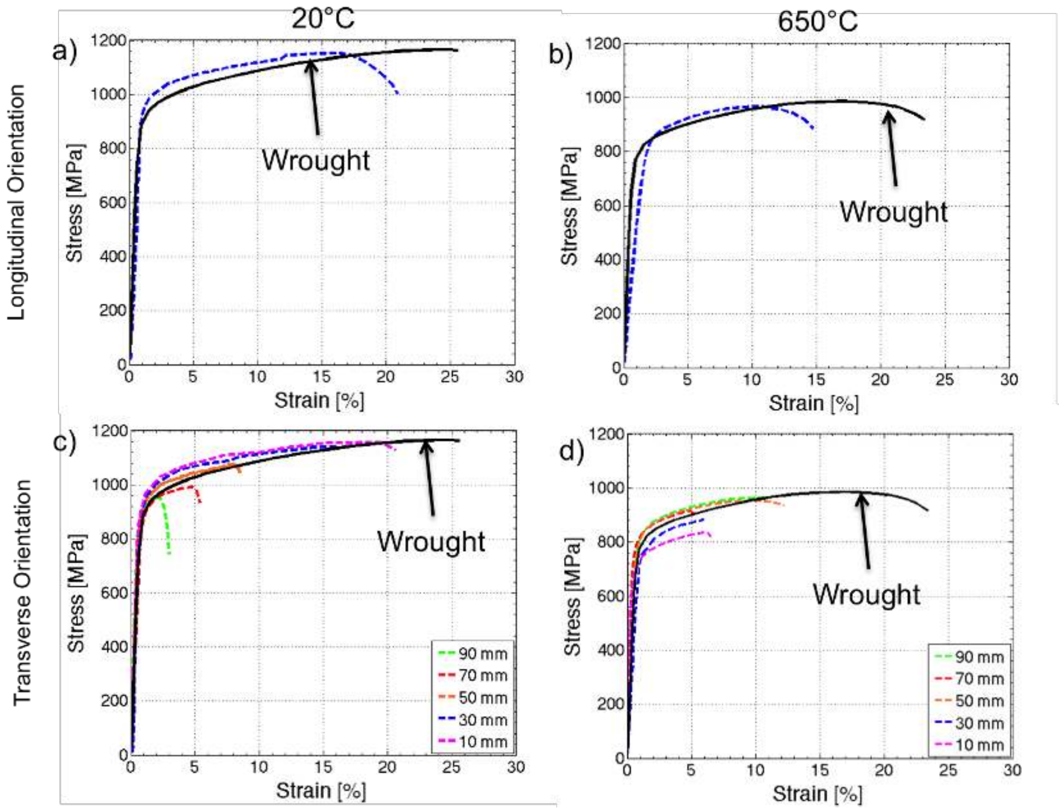

Figure 9: Tensile behavior of as-fabricated EBM Inconel 718 within the build plane and as a function of build height at a) L-orientation at room temperature b) L-orientation at 650 °C c) T-orientation at room temperature d) T-orientation at 650 °C. Reference wrought Inconel 718 behavior from [37].

After Oblak et al. [42], the relationship between yield stress and γ" volume fraction in Inconel 718 is given by the relation

$$\Delta\tau = \propto f_v^{1/2} \tag{1}$$

,where peak aged Inconel 718 is comprised of 15% γ" by volume fraction [5]. In the case of Inconel 718 tested in the as-fabricated state, the size and volume fraction of γ" is spatially dependent and a function of prior thermal history due to the decomposition mechanism $\gamma" \rightarrow \delta$. Baring the presence of porosity, the transverse tensile behavior can be directly correlated to the characteristic combination of γ" and δ. Whereas the constitutive response is a composite measure of the under aged, peak aged, and over aged microstructures.

Tabulated in Table 2 are the average tensile property values of Inconel 718 manufactured through various AM processes in the reported literature and standards. In conducting comparisons between mechanical properties reported for Inconel 718 produced via EBM and other AM methods, care must be taken to understand the reported properties in the context of their respective microstructures. As has been extensively reported, the mechanical response of Inconel 718 is sensitive to both grain size, grain structure, phase morphology and phase make-up in the wrought form [43, 44]. Further, even when processed with EBM, Inconel 718 can form different microstructures due to differences in build conditions as highlighted by those results reported in [29, 30, 37]

Table 2: Summary of reported tensile properties for Inconel 718 manufactured through additive manufacturing at room temperature in the as-fabricated state.

	Orientation	σ_y [MPa]	σ_{UT} [MPa]	ϵ_f [%]
EBM (Current Study)	L	925±20	1138±24	15.7±4.3
EBM [29]	L	822±25	1060±26	22
EBM [37]	L	669	1207	21
SLA [6]	L	830	1120	25
SLM [45]	L	995±10	1143±5	23±3
SLM [7]	L	572 ±44	904 ± 22	19±4
SLM [8]	L	849	1126	22.8
SLM [12]	L	737 ± 4	1010 ±	20.6 ±2.1
ASTM F42 As-built [46]	L	600	920	27
EBM (Current Study)	T	894±24	1061±83	11.5±6.9
EBM [29]	T	744±44	929±25	5.5
SLM [7]	T	643 ±63	991 ± 62	13±6
SLM [12]	T	816 ±24	1085±11	19.1±0.7
ASTM F42 As-built [46]	T	635	980	27

In reference to the tensile property minimums specified by ASTM F-3055 for as-fabricated Inconel 718, the EBM material reported here meet the minimum requirements for yield and ultimate strength in both the L and T-orientations. However, the ductility fell short of the minimum specifications. However, it should be noted that all ductility values reported for AM Inconel 718 in the literature fail to meet the ductility criteria of ASTM F-3055 [6–8, 29, 37, 45]. Further, the microstructure of AM Inconel 718 can most closely be related to cast Inconel 718 where AMS 5383 requires a minimum ductility of 5%.

Both Strondl et al. [29] and Unocic et al. [37] reported the as-fabricated tensile properties of EBM Inconel 718 having microstructures different than reported here. In both cases the yield strength was at least 10% below that measured in this study in the L-orientation. However, Unocic et al. the EBM

Inconel 718 which was comprised of large acicular δ needles exhibited a 5% higher ultimate strength.

Both Amato et al. [6] and Wang et al. [45] have reported on the tensile behavior of Inconel 718 fabricated through SLM. In their combined works, as-fabricated tensile results for material aligned with the build direction fell above and below those reported here. This occurrence can be attributed to the formation of the metastable Laves phase upon solidification which limits the room temperature ductility of wrought Inconel 718 [47]. In the case of EBM Inconel 718, Kirka et al. [21] reported Laves phase is only expected in the last few layers of the build; as a result the impact of the Laves phase upon the mechanical properties of EBM Inconel 718 can be considered inconsequential.

Zhao et al. [48] have shown that utilizing plasma rotating electrode processed powder over gas atomized (GA) powder results in an increase of the overall tensile properties for Inconel 718 in the HT condition while using identical laser processing conditions. The increase in the tensile behavior was attributed to a reduction in the transference of gas entrapped porosity from the GA powder to the SLM Inconel material [48]. Similarly in their work on EBM Inconel 718, Sames et al. [11] demonstrated that the resultant material was sensitive to the feedstock material. Further, Sames et al. [11] showed that the as-fabricated tensile properties are also sensitive to the rate of cool-down EBM Inconel 718 due to the associated influences on the precipitation, aging, and decomposition of γ", γ', and δ.

Illustrated in Figure 10a-d is the representative stress-strain response of post-processed EBM Inconel 718 in both the L and T-orientations in relation to reference wrought Inconel 718. Listed in Table 3 are the reported average properties within the literature for Inconel 718 processed through AM and traditional routes. Post-processing the EBM Inconel 718 material used in this study was observed to beneficially improve the tensile behavior of the material at both 20 and 650 °C and in the L and T-orientations over that of the corresponding as-fabricated material. Further, the T-orientation, post-processing reduced the variability of the ultimate strength and elongation at failure by 4x and 3x respectively in comparison to the as-fabricated material. While not typical of Inconel 718, the appearance of early strain softening at 650°C in EBM Inconel 718 is not unprecedented in Ni-base superalloys with a texture aligned along the [001] in the intermediate temperature range [49, 50].

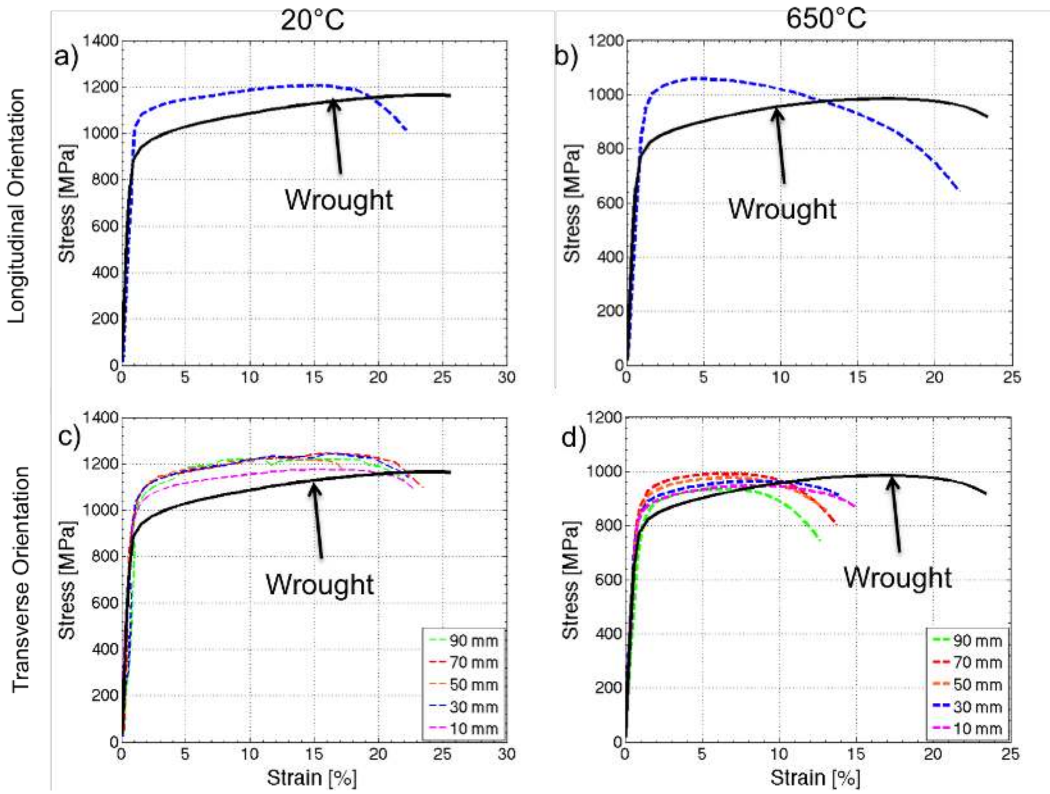

Figure 10: Tensile behavior of post-processed EBM Inconel 718 within the build plane and as a function of build height at a) L-orientation at room temperature b) L-orientation at 650 °C c) T-orientation at room temperature d) T-orientation at 650 °C. Reference wrought Inconel 718 behavior from [37].

Table 3: Summary of reported tensile properties for Inconel 718 manufactured through AM and traditional means at room temperature after post-processing.

	Orientation	σ_y [MPa]	σ_{UT} [MPa]	ϵ_f [%]
EBM HIP STA (Current Study)	L	1061±16	1266±44	21.1±1.1
EBM HT [29]	L	1154±46	1238±25	7
EBM HIP STA [37]	L	1034	1151	12.5
SLM STA [45]	L	1131±30 1319	±30	16±6
SLM HSA [8]	L	1046	1371	12.3
SLM HT [7]	L	1074 ±42	1320 ± 6	19±2
SLM HT1 [12]	L	1136 ±16	1357±5	13.6±0.2
ASTM F3055 Post-processed [46]	L	920	1240	12
EBM HIP STA (Current Study)	T	1035±17	1240±19	21.8±2.4
EBM Heat-treated [29]	T	1187±27	1232±16	1.5
SLM HT [7]	T	1159 ±32	1377 ± 66	8±6
SLM HT [12]	T	1227 ±1	1447±10	10.1±0.6
ASTM F3055 Post-processed [46]	T	940	1240	12
AMS 5383 (Cast)	–	758	802	5
AMS 5662 (Wrought)	–	1034	1241	10

Comparing the post-processed tensile properties reported here to the minimums specified by ASTM F3055 for AM Inconel 718, the yield strength and elongation at failure are exceeded for every sample tested. However when accounting for material variance, the EBM Inconel 718 in this study falls below the ASTM requirement by 20MPa. In comparison to the AMS specification for cast Inconel 718, to which the EBM microstructure can most closely be associated, the EBM material exhibits superior properties. Similarly, the EBM Inconel 718 performs favorably compared to wrought Inconel 718.

Only Strondl et al. [29] has reported on the orientation sensitivity of post-processed EBM Inconel 718 to date. In their work Strondl et al. [29] found post-processing to be beneficial as in this study, however, their material exhibited inferior ductility to their as-fabricated material. This can largely be attributed to the presence of porosity aligned with the grain boundaries and the lack of a HIP treatment given to the material [29]. The behavior of HIP+STA EBM Inconel 718 reported by Unocic et al. [37] showed similar improvements in the strength values of EBM Inconel 718. However, Unocic et al. [37] reported the tested microstructure as having undergone significant grain growth and potentially impacting the ductility of the material. In comparison to post-processed Inconel 718 manufactured through laser processes, EBM Inconel 718 exhibits superior ductility, with the yield strengths being largely similar, however, σ_{UT} is generally 10 % below that of laser processed Inconel 718. However, a direct comparison of the results reported within the literature is difficult due to each being fabricated under different conditions and being given unique post-processing steps.

To adequately optimize the tensile behavior of EBM Inconel 718, investigative studies on the effect of post-processing parameters is required. For example, Rao et al. [51] in their investigation of post-processing parameters on the tensile properties of Inconel 718 powder compact was most sensitive to the supersolvus solutioning temperature. Utilizing solution temperatures in the range of 1000-1200 °C were observed to maximize the properties of the Inconel 718 powder compact. However, as has been shown through comparing reported Inconel 718 results from reported studies, the resultant microstructure and tensile behavior is highly sensitive to the conditions under which the material fabricated even when the same AM process is used [7, 8, 29, 30, 37, 45]. Further, distinguishing characteristics of AM fabricated Inconel 718 such as δ precipitate size and morphology and grain size are not direct predictors of the materials performance under tensile loading as can be reasoned from the property summaries in Tables 2-3.

4 Conclusions

Investigated in this work is the effect of Inconel 718 microstructue on the tensile properties of material in the as-fabricated and post-processed states. While the results presented are in the context of a specific build, the general trends and observations can be considered to hold true for EBM Inconel 718 builds. The results presented here can be generalized as follows:

- EBM Inconel 718 in the as-fabricated state exhibits a spatially dependent microstructure sensitive to the height of the build. The spatially dependent microstructure is due to temporal and thermal exposure of the Inconel 718 during the build process.
- Post-processing of EBM Inconel 718 consisted of two steps: 1) HIP treatment to remove porosity 2) Solution treating and precipitate aging. Post-processing of the EBM Inconel 718 homogenized the precipitate structure while retaining the columnar grain structure.
- As-built EBM Inconel 718 exhibits a tensile property sensitivity to the build height in the T-orientation at both 20 and 650 °C. Within the L-orientation the material behaves in a uniform manner. Variations in ϵ_f observed in both the L and T-orientation are attributable to the presence of porosity in the material.

- Post-processing EBM Inconel 718 preferentially enhances the mechanical properties in both directions and at room temperature and 650 °C. Additionally, post-processing decreases the spatial variance of the ultimate yield strength and elongation at failure within the T-orientation by factors of 4 and 3 respectively.

5 Acknowledgements

This research sponsored by the US Department of Energy, Office of Energy Efficiency and Renewable Energy, Advanced Manufacturing Office, under contract DE-AC05-00OR22725 with UT-Battelle, LLC.

6 References

[1] Wagner, H. J., and Hall, A. M., 1965. *Physical Metallurgy of Alloy 718*. Tech. rep., Battelle Memorial Institue.

[2] Preli, F. R., and Furrer, D., 2014. "*Lessons Learned From The Development, Application And Advancement Of Alloy 718*". In 8th International Symposium on Superalloy 718 and Derivatives, E. Ott, A. Banik, X. Liu, K. H. Ian Dempster, J. Andersson, J. Groh, T. Gabb, R. Helmink, and A. Wusatowska-Sarnek, eds., pp. 3–14.

[3] Brooks, J. W., and Bridges, P. J., 1988. "*Metallurgical Stability of Inconel 718 Alloys*". In Superalloys 1988, S. Reichman, D. Duhl, G. Maurer, S. Antolovich, and C. Lund, eds., pp. 33–42.

[4] Loria, E. A., 1988. "*The Status and Prospects of Alloy 718*". *JOM,* **40**(7), pp. 36–41.

[5] Chaturvedi, M. C., and Han, Y.-f., 1983. "*Strengthening mechanisms in Inconel 718 superalloy*". *Metal Science,* **17**(3), pp. 145–149.

[6] Amato, K., Gaytan, S., Murr, L., Martinez, E., Shindo, P., Hernandez, J., Collins, S., and Medina, F., 2012. "*Microstructures and mechanical behavior of Inconel 718 fabricated by selective laser melting*". *Acta Materialia,* **60**(5), pp. 2229 – 2239.

[7] Chlebus, E., Gruber, K., Kuźnicka, B., Kurzac, J., and Kurzynowski, T., 2015. "*Effect of heat treatment on the microstructure and mechanical properties of Inconel 718 processed by selective laser melting*". *Materials Science and Engineering: A,* **639**, pp. 647 – 655.

[8] Zhang, D., Niu, W., Cao, X., and Liu, Z., 2015. "*Effect of standard heat treatment on the microstructure and mechanical properties of selective laser melting manufactured Inconel 718 superalloy*". *Materials Science and Engineering: A,* **644**, pp. 32 – 40.

[9] Sames, W., Unocic, K., Dehoff, R., Lolla, T., and Babu, S., 2014. "*Thermal Effects on Microstructural Heterogeneity of Inconel 718 Materials Fabricated by Electron Beam Melting*". *Journal of Materials Research,* **29**, pp. 1920–1930.

[10] Tian, Y., McAllister, D., Colijn, H., Mills, M., Farson, D., Nordin, M., and Babu, S., 2014. "*Rationalization of Microstructure Heterogeneity in INCONEL 718 Builds Made by the Direct Laser Additive Manufacturing Process*". *Metallurgical and Materials Transactions A,* **45**(10), pp. 4470–4483.

[11] Sames, W., Medina, F., Peter, W., Babu, S., and Dehoff, R., 2014. "*Effect of Process Control and Powder Quality on Inconel 718 Produced Using Electron Beam Melting*". In 8th International Symposium on Superalloy 718 and Derivatives.

[12] Strößner, J., Terock, M., and Glatzel, U., 2015. "*Mechanical and Microstructural Investigation of Nickel-Based Superalloy IN718 Manufactured by Selective Laser Melting (SLM)*". *Advanced Engineering Materials,* **17**(8), pp. 1099–1105.

[13] , February 7, 2016. *http://www.arcam.com/*. Tech. rep.

[14] , 2007. *Inconel alloy 718*. Tech. Rep. SMC-045, Special Metals Corporation.

[15] , 2013. *ASTM E08-13a Standard Test Methods for Tension Testing of Metallic Materials*. Tech. rep., ASTM International.

[16] , 2009. *ASTM E21-09 Standard Test Methods for Elevated Temperature Tension Tests of Metallic Materials*. Tech. rep., ASTM International.

[17] Gäumann, M., Henry, S., Cléton, F., Wagnière, J. D., and Kurz, W., 1999. "*Epitaxial laser metal forming: analysis of microstructure formation*". *Materials Science and Engineering: A,* **271**(1-2), pp. 232–241.

[18] Kurz, W., and Fisher, D. J., 1992. *Fundamentals of Solidification*, 3rd ed. Trans Tech Publications.

[19] Helmer, H. E., Körner, C., and Singer, R. F., 2014. "*Additive manufacturing of nickel-based superalloy Inconel 718 by selective electron beam melting: Processing window and microstructure*". *Journal of Materials Research,* **29**, pp. 1987–1996.

[20] Makiewicz, K., 2013. "*Development of Simultaneous Transformation Kinetics Microstructure Model with Application to Laser Metal Deposited Ti-6Al-4V and Alloy 718*". Master's thesis, The Ohio State University.

[21] Kirka, M. M., Unocic, K., Raghavan, N., Medina, F., Dehoff, R. R., and Babu, S. S., 2016. "*Microstructure Development in Electron Beam Melted Inconel 718 and Associated Tensile Properties*". *Journal of Materials*.

[22] Devaux, A., Nazé, L., Molins, R., Pineau, A., Organista, A., Guédou, J., Uginet, J., and Héritier, P., 2008. "*Gamma Double Prime Precipitation Kinetic in Alloy 718*". *Materials Science and Engineering: A,* **486**(1-2), pp. 117–122.

[23] Carlson, R., and Radavich, J., 1989. "*Microstructural Chraterization of Cast 718*". In Superalloy 718: metallurgy and applications, E. Loria, ed., Minerals, Metals & Materials Society, pp. 79–95.

[24] Muralidharan, G., Thompson, R., and Walck, S., 1989. "*Analysis of precipitation in cast alloy 718*". *Ultramicroscopy,* **29**(1–4), pp. 277 – 283.

[25] Knorovsky, G., Cieslak, M., Headley, T., Romig, A., and Hammetter, W., 1989. "*INCONEL 718: A solidification diagram*". *Metallurgical Transactions A,* **20**(10), pp. 2149–2158.

[26] Liang, X., Zhang, R., Yang, Y., and Han, Y., 1994. "*An Investigation of the Homogenization and Deformation of Alloys 718 Ingots*". In Superalloys 718,625,706 and Various Derivatives, E. Loria, ed., pp. 947–956.

[27] Huang, X., Chaturvedi, M. C., and Richards, N. L., 1996. "*Effect of homogenization heat treatment on the microstructure and heat- affected zone microfissuring in welded cast alloy 718*". *Metallurgical and Materials Transactions A,* **27**(3), pp. 785–790.

[28] jun MIAO, Z., dang SHAN, A., biao WU, Y., LU, J., liang XU, W., and wei SONG, H., 2011. "*Quantitative analysis of homogenization treatment of {INCONEL718} superalloy*". *Transactions of Nonferrous Metals Society of China,* **21**(5), pp. 1009 – 1017.

[29] Strondl, A., Palm, M., Gnauk, J., and Frommeyer, G., 2011. "*Microstructure and mechanical properties of nickel based superalloy IN718 produced by rapid prototyping with electron beam melting (EBM)*". *Materials Science and Technology,* **27**(5), pp. 876–883.

[30] Strondl, A., Fischer, R., Frommeyer, G., and Schneider, A., 2008. "*Investigations of {MX} and / Precipitates in the Nickel-based Superalloy 718 Produced by Electron Beam Melting*". *Materials Science and Engineering: A,* **480**, pp. 138–147.

[31] Azadian, S., Wei, L.-Y., and Warren, R., 2004. "*Delta phase precipitation in Inconel 718*". *Materials Characterization,* **53**(1), pp. 7 – 16.

[32] Radavich, J. F., 1989. "*The Physical Metallurgy of Cast and Wrought Alloy 718*". In Superalloy 718: metallurgy and applications, E. Loria, ed., Minerals, Metals & Materials Society, pp. 229–240.

[33] Sames, W. J., 2015. "*Additive Manufacturing Of Inconel 718 Using Electron Beam Melting: Processing, Post-Processing, and Mechanical Properties*". PhD thesis, Texas A&M University.

[34] Sims, C., 1972. *The Superalloys*. John Wiley and Sons.

[35] Raymond, E. L., 1989. "*Effect of Chemistry and Processing on the Structure and Mecanical Properties of Inconel Alloy 718*". In Superalloy 718: metallurgy and applications, E. Loria, ed., Minerals, Metals & Materials Society.

[36] Bouse, G. K., and Behrendt, M. R., 1997. "*Mechanical Properties of Fine-Grain Microcast-X Alloy 718 Investment Castings for SSME, Gas Turbine Engine, and Airframe Components*". In *Superalloys 718, 625 and Various Derivatives*, E. A. Loria, ed. pp. 319–328.

[37] Unocic, K. A., Kolbus, L. M., Dehoff, R. R., Dryepondt, S. N., and Pint, B. A., 2014. "*High Temperature Performance of UNS N07718 Processed by Additive Manufacturing*". In Corrosion, NACE International.

[38] Miracle, D., Committee, A. I. H., and Donaldson, S., 2001. *ASM Handbook*. No. v. 4 in ASM Handbook. ASM International.

[39] Sochalski-Kolbus, L., Payzant, E., Cornwell, P., Watkins, T., Babu, S., Dehoff, R., Lorenz, M., Ovchinnikova, O., and Duty, C., 2015. "*Comparison of Residual Stresses in Inconel 718 Simple Parts Made by Electron Beam Melting and Direct Laser Metal Sintering*". *Metallurgical and Materials Transactions A,* **46**(3), pp. 1419–1432.

[40] Cai, D., Zhang, W., Nie, P., Liu, W., and Yao, M., 2007. "*Dissolution kinetics of phase and its influence on the notch sensitivity of Inconel 718*". *Materials Characterization,* **58**(3), pp. 220 – 225.

[41] Qi, H., Azer, M., and Ritter, A., 2009. "*Studies of Standard Heat Treatment Effects on Microstructure and Mechanical Properties of Laser Net Shape Manufactured INCONEL 718*". *Metallurgical and Materials Transactions A,* **40**(10), pp. 2410–2422.

[42] Oblak, J. M., Paulonis, D. F., and Duvall, D. S., 1974. "*Coherency Strengthening in Ni Base Alloys Hardened by* $D0_{22}$ γ'' *Precipitates*". *Metallurgical and Materials Transactions,* **5**, pp. 143–154.

[43] Tien, J., and Caulfield, T., eds., 1989. *Superalloys, Supercomposites, and Superceramics*. Academic Press.

[44] Lasalmonie, A., and Strudel, J. L., 1986. "*Influence of grain size on the mechanical behaviour of some high strength materials*". *Journal of Materials Science,* **21**(6), pp. 1837–1852.

[45] Wang, Z., Guan, K., Gao, M., Li, X., Chen, X., and Zeng, X., 2012. "*The microstructure and mechanical properties of deposited-IN718 by selective laser melting*". *Journal of Alloys and Compounds,* **513**(0), pp. 518 – 523.

[46] , 2014. *ASTM F305514a Standard Specification for Additive Manufacturing Nickel Alloy (UNS N07718) with Powder Bed Fusion*. Tech. rep., ASTM International.

[47] Schirra, J. J., Caless, R. H., and Hatala, R. W., 1991. "*The Effect of Laves Phase on the Mechanical Properties of Wrought and Cast+HIP Inconel 718*". In Superalloys 718, 625 and Various Derivatives, E. A. Loria, ed., pp. 375–388.

[48] Zhao, X., Chen, J., Lin, X., and Huang, W., 2008. "*Study on microstructure and mechanical properties of laser rapid forming Inconel 718*". *Materials Science and Engineering: A,* **478**(1–2), pp. 119 – 124.

[49] Cahn, R., and Haasen, P., 1996. *Physical Metallurgy*. No. v. 1 in Physical metallurgy. Elsevier Science.

[50] Caron, P., and Khan, T., 1987. "*Tensile Behaviour of a Nickel-based Single Crystal Superalloy: Effects of Temperature and Orientation*". In Advanced Materials and Processing Techniques for Structural Applications: 1st Technical Conference : Papers, T. Khan and A. Lasalmonie, eds., Office National d'Etudes et de Recherches Aerospatiales, pp. 59–70.

[51] Rao, G. A., Srinivas, M., and Sarma, D., 2004. "*Effect of Solution Treatment Temperature on Microstructure and Mechanical Properties of Hot Isostatically Pressed Superalloy Inconel 718*". *Materials Science and Technology,* **20**(9), pp. 1161–1170.

List of Tables

List of Figures